Overcoming CAR-Mediated CD19 Downmodulation and Leukemia Relapse with T Lymphocytes Secreting Anti-CD19 T-cell Engagers

Belén Blanco[1,2,3], Ángel Ramírez-Fernández[1,2], Clara Bueno[3,4,5], Lidia Argemí-Muntadas[6], Patricia Fuentes[7], Óscar Aguilar-Sopeña[8,9], Francisco Gutierrez-Agüera[3,4], Samanta Romina Zanetti[4], Antonio Tapia-Galisteo[10], Laura Díez-Alonso[1,2], Alejandro Segura-Tudela[1,2], Maria Castellà[11], Berta Marzal[11], Sergi Betriu[11], Seandean L. Harwood[6], Marta Compte[10], Simon Lykkemark[6], Ainhoa Erce-Llamazares[1,2], Laura Rubio-Pérez[1,2,12], Anaïs Jiménez-Reinoso[1,2], Carmen Domínguez-Alonso[1,2], Maria Neves[7], Pablo Morales[1], Estela Paz-Artal[1,8], Sonia Guedan[13], Laura Sanz[10], María L. Toribio[7], Pedro Roda-Navarro[8,9], Manel Juan[11,14,15,16], Pablo Menéndez[3,4,5,17,18], and Luis Álvarez-Vallina[1,2,3,6]

ABSTRACT

Chimeric antigen receptor (CAR)–modified T cells have revolutionized the treatment of CD19-positive hematologic malignancies. Although anti-CD19 CAR-engineered autologous T cells can induce remission in patients with B-cell acute lymphoblastic leukemia, a large subset relapse, most of them with CD19-positive disease. Therefore, new therapeutic strategies are clearly needed. Here, we report a comprehensive study comparing engineered T cells either expressing a second-generation anti-CD19 CAR (CAR-T19) or secreting a CD19/CD3-targeting bispecific T-cell engager antibody (STAb-T19). We found that STAb-T19 cells are more effective than CAR-T19 cells at inducing cytotoxicity, avoiding leukemia escape *in vitro*, and preventing relapse *in vivo*. We observed that leukemia escape *in vitro* is associated with rapid and drastic CAR-induced internalization of CD19 that is coupled with lysosome-mediated degradation, leading to the emergence of transiently CD19-negative leukemic cells that evade the immune response of engineered CAR-T19 cells. In contrast, engineered STAb-T19 cells induce the formation of canonical immunologic synapses and prevent the CD19 downmodulation observed in anti-CD19 CAR-mediated interactions. Although both strategies show similar efficacy in short-term mouse models, there is a significant difference in a long-term patient-derived xenograft mouse model, where STAb-T19 cells efficiently eradicated leukemia cells, but leukemia relapsed after CAR-T19 therapy. Our findings suggest that the absence of CD19 downmodulation in the STAb-T19 strategy, coupled with the continued antibody secretion, allows an efficient recruitment of the endogenous T-cell pool, resulting in fast and effective elimination of cancer cells that may prevent CD19-positive relapses frequently associated with CAR-T19 therapies.

Introduction

Potentially curative immunotherapies for B-cell leukemias have been based on redirecting the specificity and function of non-tumor-specific T cells with synthetic CD19-targeted cell–cell bridging molecules, such as membrane-anchored chimeric antigen receptors (CAR) or soluble bispecific antibodies (bsAb; ref. 1). Administration of anti-CD19 CAR-engineered autologous T (CAR-T19) cells and continuous infusion of the anti-CD19/CD3 bispecific T-cell engager (BiTE) blinatumomab (BLI) have demonstrated impressive complete

[1]Cancer Immunotherapy Unit (UNICA), Department of Immunology, Hospital Universitario 12 de Octubre, Madrid, Spain. [2]Immuno-Oncology and Immunotherapy Group, Instituto de Investigación Sanitaria 12 de Octubre (imas12), Madrid, Spain. [3]Red Española de Terapias Avanzadas (TERAV), Instituto de Salud Carlos III (RICORS, RD21/0017/0029), Madrid, Spain. [4]Josep Carreras Leukemia Research Institute, Barcelona, Spain. [5]Centro de Investigación Biomédica en Red-Oncología (CIBERONC), Instituto de Salud Carlos III, Madrid, Spain. [6]Immunotherapy and Cell Engineering Laboratory, Department of Engineering, Aarhus University, Aarhus, Denmark. [7]Centro de Biología Molecular Severo Ochoa CSIC-UAM, Madrid, Spain. [8]Department of Immunology, Ophthalmology and ENT, School of Medicine, Universidad Complutense, Madrid, Spain. [9]Lymphocyte Immunobiology Group, Instituto de Investigación Sanitaria 12 de Octubre (imas12), Madrid, Spain. [10]Molecular Immunology Unit, Hospital Universitario Puerta de Hierro Majadahonda, Majadahonda, Madrid, Spain. [11]Institut d'Investigacions Biomèdiques August Pi i Sunyer (IDIBAPS), Hospital Clínic, Barcelona, Spain. [12]Chair for Immunology UFV/Merck, Universidad Francisco de Vitoria (UFV), Pozuelo de Alarcón, Madrid, Spain. [13]Department of Hematology and Oncology, Institut d'Investigacions Biomèdiques August Pi i Sunyer (IDIBAPS), Hospital Clinic, Barcelona, Spain. [14]Servei d'Immunologia, Hospital Clínic de Barcelona, Barcelona, Spain. [15]Plataforma Immunoteràpia Hospital Sant Joan de Déu, Barcelona, Spain. [16]Universitat de Barcelona, Barcelona, Spain. [17]Department of Biomedicine, School of Medicine, Universitat de Barcelona, Barcelona, Spain. [18]Institució Catalana de Recerca i Estudis Avançats (ICREA), Barcelona, Spain.

Note: Supplementary data for this article are available at Cancer Immunology Research Online (http://cancerimmunolres.aacrjournals.org/).

B. Blanco and Á. Ramírez-Fernández contributed equally to this article.

Current address for M. Neves: Division of Clinical Genetics, Lund University, Lund 22184, Sweden.

Corresponding Authors: Luis Álvarez-Vallina, Cancer Immunotherapy Unit, Hospital Universitario 12 De Octubre, Madrid 28041, Spain. Phone: 34-917792773; Fax: 34-917792778; E-mail: lav.imas12@h12o.es; and Belén Blanco, bblanco.imas12@h12o.es

Cancer Immunol Res 2022;10:498–511

doi: 10.1158/2326-6066.CIR-21-0853

response rates in refractory/relapsed B-cell acute lymphoblastic leukemia (B-ALL; refs. 2, 3). However, despite this excellent clinical performance, disease recurrence/progression is eventually seen in 30% to 60% of patients after CAR-T19 cell therapy (4, 5). Relapses fall under two major types: CD19-positive (70%–80% of patients), typically linked to poor T-cell function, limited CAR T-cell persistence, and an overall low redirection of T cells (6), and CD19-negative (20%–30% of patients), where the disease recurs with antigen-negative variants enabling escape from CAR-T19 surveillance (4, 7). CAR-T19 therapy can also lead to reversible antigen loss through trogocytosis, a mechanism by which targeted antigens are transferred to T cells, thereby reducing both CD19 density on the tumor cell surface and CAR expression on T cells, resulting in T-cell fratricide and exhaustion (8). Approved CAR T-cell therapies rely on stable cell-surface CAR expression, whereas BiTE-mediated T-cell redirection is temporary and limited to the period of systemic infusion. As an alternative to BiTE infusion, T cells can be engineered to continuously secrete T cell–engaging bsAbs (STAb T cells) in order to compensate for their rapid blood clearance and achieve long-term therapeutically effective concentrations (9, 10). STAb T-cell therapy is under active preclinical investigation as an alternative to CAR T cells, and several groups have demonstrated encouraging therapeutic effects in preclinical models of B-ALL (11, 12). Here, we report a comparative study aimed at determining the efficacy of CD19-targeting engineered CAR T and STAb T cells in several *in vitro* and *in vivo* models of B-ALL. Although our results indicate that STAb-T19 therapy effectively controls tumor progression and can prevent the relapse frequently associated with CAR-T19 therapies in different *in vivo* models, further studies are needed to determine its ultimate clinical potential.

Materials and Methods

Cell lines and culture conditions

HEK293 (CRL-1573), HEK293T (CRL-3216), HeLa (CCL-2), Jurkat Clone E6-1 (TIB-152), Raji (CCL-86), NALM6 (CRL3273), and K562 (CCL-243) cells were obtained from the American Type Culture Collection. SEM (ACC546) cells were obtained from the DSMZ cell line bank. NALM6 and HeLa cells expressing the firefly luciferase (Luc) gene ($NALM6^{Luc}$ and $HeLa^{Luc}$) have been described previously (13). HEK293, HEK293T, and HeLa cells were cultured in Dulbecco's modified Eagle medium (DMEM; catalog no. BE12-614F, Lonza) supplemented with 2 mmol/L L-glutamine (catalog no. 25030081, Life Technologies), 10% (vol/vol) heat-inactivated FBS (catalog no. F7524) and antibiotics (100 units/mL penicillin, 100 μg/mL streptomycin; catalog no. P4333; both from Sigma-Aldrich), referred to as DMEM complete medium. Jurkat, Raji, Nalm6, and K562 cells were cultured in RPMI-1640 (catalog no. 12-702Q, Lonza) supplemented with 2 mmol/L L-glutamine, heat-inactivated 10% FBS, and antibiotics, referred to as RPMI complete medium (RCM). SEM cells were cultured in Iscove's Modified Dulbecco's Medium (catalog no. 31980030, Thermo Fisher Scientific) supplemented with heat-inactivated 10% FCS and antibiotics. All the cell lines were grown at 37°C in 5% CO_2 for no longer than 1 month during experimental use and were routinely screened for mycoplasma contamination by PCR using the Mycoplasma Gel Detection Kit (catalog no. 90.021-4542, Biotools). Primary human B-ALL cells ($n = 3$) were obtained from patients' bone marrow (BM) samples after written informed consent, and the study was conducted in accordance with the Declaration of Helsinki. Mononuclear cells were isolated from BM samples by density gradient centrifugation using Ficoll-Paque (catalog no. 17-5446-52, Cytiva), washed, resuspended in FBS with 10% DMSO (catalog no. 317275, EMD Millipore) and stored in liquid nitrogen until use. B-ALL1 sample was an ETV6-RUNX1 t(12;21) B-ALL, and B-ALL2 sample a hypodiploid B-ALL. The sample used for generation of patient-derived xenograft (PDX) model was a high hyperdiploid B-ALL, obtained from the BM of a 3-year-old patient at diagnosis (prior to treatment) and blasts were sequentially expanded in NSG mice. Briefly, mice injected with 1×10^6 B-ALL cells were allowed to reach 85% blasts in BM. Then, mice were sacrificed, and blasts were obtained from tibiae and femurs and cryopreserved in FBS–10% DMSO until use.

Vector construction and preparation of lentivirus

To construct the expression vector pCDNA3.1-A3B1-OKT3, a synthetic gene (19-BiTE) encoding the human kappa light chain signal peptide L1 (14), the A3B1 scFv (V_L–V_H; ref. 13), a five-residue linker (G_4S), the OKT3 scFv (V_H–V_L; ref. 15), and a C-terminal polyHis tag was synthesized by GeneArt AG (Thermo Fisher Scientific), and subcloned as *Hind*III/*Xba*I into the plasmid pCDNA3.1 (catalog no. V79520, Thermo Fisher Scientific), using T4 DNA ligase (catalog no. M0202S, New England Biolabs). To generate the lentiviral transfer vector, the complete 19-BiTE gene (including signal peptide L1, A3B1 scFv (G_4S), OKT3 scFv, and polyHis tag) was synthesized by GeneArt AG and cloned as *Mlu*I/*BspE*I into the vector pCCL-EF1α-CAR19 (13), encoding a second-generation (CD8-BBζ) anti-CD19 CAR (19-CAR), to obtain the plasmid pCCL-EF1α-BiTE19. To construct the vector pCCL-EF1α-BiTE19-T2A-Tomato, a synthetic gene encoding the OKT3 scFv and T2A-Tomato was synthesized by GeneArt AG, and cloned as *Afe*I/*Bst*BI into the vector pCCL-EF1α-BiTE19. The plasmid pCCL-EF1α-CAR19-T2A-GFP has been previously described (16).

Lentivirus titration

All lentivirus stocks were normalized for p24 and RNA. The p24 concentration was determined by ELISA (catalog no. 632200, Takara), and the genomic lentiviral RNA by qRT-PCR (catalog no. 631235, Takara). In the case of 19-BBζ CAR-encoding lentivirus, functional titers (TU/mL) were determined by FACS analysis after limiting dilution in HEK293T cells, using an APC-conjugated $F(ab')_2$ fragment goat anti-mouse IgG $F(ab')_2$ fragment specific (catalog no. 115-006-072, Jackson ImmunoResearch Laboratories). Titration of 19-BiTE lentiviral preparations was performed by intracellular staining, as described below, of HEK293T cells after limiting dilution. Functional titers of 19-BBζ CAR and 19-BiTE-encoding lentiviruses carrying reporter genes were determined by flow cytometry by analyzing green fluorescence protein (GFP) or dTomato (dTO) expression, respectively, after limiting dilution in HEK293T cells.

T-cell transduction and culture conditions

Peripheral blood mononuclear cells (PBMC) were isolated from peripheral blood of volunteer healthy donors ($n = 15$) by density gradient centrifugation using lymphoprep (catalog no. AXS-1114544, Axis–Shield). All donors provided written informed consent in accordance with the Declaration of Helsinki. $CD3^+$ T cells were purified by negative selection using the Pan T-Cell Isolation Kit, human (catalog no. 130-096-535), and LS columns (catalog no. 130-042-401; both from Miltenyi Biotec, following the manufacturer's instructions. The purity of isolated populations was routinely >95%. Cells were then activated and expanded for 24 hours using anti-CD3/CD28 beads (catalog no. 111.31D, Dynabeads, Gibco) at 1:3 cell:bead ratio in RCM, at a concentration of 1×10^6 cells/mL. Twenty-four hours later, cells were left nontransduced (NT cells) or transduced with 19-CAR (CAR T cells) or 19-BiTE (STAb T cells) encoding lentiviruses at the indicated MOIs. A period of cell expansion of 6 to 8 days was necessary

before conducting experiments. Three different cell transductions using three different PBMC donors were used to conduct the experiments in triplicate. Alternatively, PBMCs obtained from Buffy coats provided by the Barcelona Blood and Tissue Bank on institutional review board approval (HCB/2018/0030) were activated in plates coated with 1 μg/mL anti-CD3 (OKT3; catalog no. 566685) and anti-CD28 (CD28.2; catalog no. 555725) antibodies (BD Biosciences) for 2 days and then were transduced with 19-BBζ CAR (CAR-T19 cells) or 19-BiTE (STAb-T19 cells) encoding lentiviruses at the indicated MOIs in the presence of 10 ng/mL IL7 (catalog no. 30-095-367) and 10 ng/mL IL15 (catalog no. 130-095-760; both from Miltenyi Biotec). T cells were expanded in RCM supplemented with IL7 and IL15 (10 ng/mL; Miltenyi Biotec) for up to 10 days.

Western blotting

Samples were separated under reducing conditions on 10% to 20% Tris-glycine gels (catalog no. XP10202BOX, Life Technologies), transferred onto PVDF membranes (catalog no. IPVH00010, Merck Millipore) and probed with anti-His mAb (catalog no. 34650, Qiagen; 200 ng/mL), followed by incubation with horseradish peroxidase (HRP)–conjugated goat anti-mouse (GAM) IgG, Fc specific (1:5,000 dilution; Sigma-Aldrich, see Supplementary Table S1). Visualization of protein bands was performed with Pierce ECL Western Blotting substrate (catalog no. 32134).

Enzyme-linked immunosorbent assay

To detect the 19-BiTE secreted to culture supernatants, human CD19:human Fc chimera (CD19:Fc; catalog no. 9269-CD-050, R&D Systems) was immobilized (5 μg/mL) on Maxisorp plates (catalog no. M9410-1CS, NUNC) overnight at 4°C. After washing and blocking, conditioned media were added and incubated for 1 hour at room temperature. Then, wells were washed 3 times with PBS–0.05% Tween20 (catalog no. P1379, Sigma-Aldrich) and 3 times with PBS (catalog no. 508002, Werfen), and anti-His mAb (Qiagen) was added (1 μg/mL). After washing, HRP-GAM IgG, Fc specific (1:2,000 dilution; Sigma-Aldrich) was added, and the plate was developed using tetramethylbenzidine (TMB; catalog no. T0440, Sigma-Aldrich).

T-cell proliferation assays

For primary T-cell proliferation assays, anti-CD3/CD28 beads were removed five days after lentiviral transduction, and activated T cells (A-T) were left resting for 24 hours at a concentration of 0.8×10^6 cells/mL. Then, transduced or nontransduced A-T were stained with 2.5 μmol/L Cell Trace Violet (catalog no. C34557, Life Technologies) and cocultured with freshly isolated T cells (nonactivated T cells, NA-T) from the same donor, previously stained with 2.5 μmol/L Cell Trace CFSE (catalog no. C34554, Life Technologies), and NALM6 or HeLa target cells at the indicated ratios. After 5 days, samples were stained with CD3-PE, CD4-APC, and CD8-APC-Cy7 (all from BD Biosciences; see Supplementary Table S1) and acquired in a FACSCanto flow cytometer. T-cell proliferation was analyzed using FCS Express 6 Plus Software (De Novo Software).

Cytokine secretion analysis

IFNγ secretion was analyzed by ELISA (catalog no. 950.000.096, Diaclone), following the manufacturer's instructions.

Cytotoxicity assays

For 48-hour cytotoxicity assays, transduced or nontransduced A-T cells were cocultured with or without freshly isolated NA-T cells and luciferase-expressing target cells ($NALM6^{Luc}$ or $HeLa^{Luc}$) at the indicated effector-to-target (E:T) ratios. As controls, NA-T cells were cultured with target cells. After 48 hours, supernatants were collected and stored at −20ºC for IFNγ secretion analysis, and 20 μg/mL D-luciferin (catalog no. E1602, Promega) was added before bioluminescence quantification using a Victor luminometer (PerkinElmer). Percent tumor cell viability was calculated as the mean bioluminescence of each sample divided by the mean of NA-T-target cell samples ×100. Specific lysis was established as 100% of cell viability. For cytotoxic studies using transwells, polycarbonate inserts (0.4 μmol/L pores; catalog no. CLS3381-1EA, Corning) were used. Luciferase-expressing targets cells (5×10^4) were plated on bottom wells with 1×10^5 NA-T cells, and A-T cells were added at the indicated ratios to inserts. Bioluminescence was quantified after 48 hours. In another set of experiments, transduced or nontransduced A-T cells were cocultured with or without freshly isolated NA-T cells and 1×10^5 tumor target cells (NALM6, SEM, or primary B-ALL cells) at the indicated E:T ratios. After 24 and 48 hours, cells were stained for 30 minutes at 4°C with CD3-PB, CD10-APC, CD19-PCy7, and 7-AAD (catalog no. 559925, BD Biosciences) in 50 μL PBS–0.5% FBS, in TruCount Absolute Counting Tubes (catalog no. 340334, BD Biosciences). Then, samples were diluted by adding 450 μL of PBS and gently mixed before proceeding to FACS analysis. Cytotoxicity was determined by analyzing the residual live (7-AAD^-) target cells. For real-time cytotoxicity assays, the xCELLigence RTCA DP system (Acea Biosciences) was used. 1×10^4 wild-type HEK293 or stably transfected CD19-expressing HEK293 cells were plated in an E-Plate 16 (catalog no. 05469813001, Acea Biosciences) and cultured at 37 °C and 5% CO_2. After 20 hours, NT-T, CAR-T19 or STAb-T19 cells were added at different E:T ratios and cell index values were measured every 15 minutes for 48 hours using RTCA Software 2.0 (Acea Biosciences). The percentage of specific lysis was calculated using the equation:

$$\text{Percentage} = [(\text{cell index of NT} - \text{cell index of CAR T cells})/(\text{cell index of NT})] \times 100$$

CD107a assays

NT-T, CAR-T19, or STAb-T19 cells (1×10^5) were cultured alone or coincubated with NALM6 or HeLa cells at a 2:1 E:T ratio in U-bottom 96-well plates, in the presence of anti-human CD107a-PE (BD Biosciences, see Supplementary Table S1). After 1 hour, 0.67 μL/mL monensin (BD GolgiStop, catalog no. 554724, BD Biosciences) was added, and cultures were continued for another 3 hours before CD3 staining and flow-cytometric analysis.

Flow cytometry

Antibodies used for flow cytometry analysis are detailed in Supplementary Table S1. DAPI (catalog no. D9542-10MG, Sigma-Aldrich) and 7-Aminoactinomycin D (7-AAD; cat. 559925, BD Biosciences) were used as viability markers. Cell-surface expression of 19-CAR was analyzed using an APC-anti-mouse IgG $F(ab')_2$; alternatively, CAR expression was estimated based on GFP expression. Cell surface–bound 19-BiTEs were detected with 1 μg/mL anti-6xHis tag-biotin mAb and PE-conjugated streptavidin (cat. 349023, BD Biosciences), or with APC-conjugated anti-His mAb. Intracellular 19-BiTE was detected using the Inside Stain Kit (cat. 130-090-477, Miltenyi Biotec) following the manufacturer's instructions, and APC-anti-His APC mAb. Alternatively, 19-BiTE was estimated based on dTO expression. Intracellular CD19 was detected using the Inside Stain Kit and PC5-conjugated anti-CD19 mAb. Cell acquisition was performed in a BD FACSCAnto II flow cytometer using BD FACSDiva software (both from BD Biosciences). Analysis was performed using FlowJo V10 software (Tree Star).

Immunofluorescence and confocal microscopy

Antibodies used for immunofluorescence and confocal microscopy analysis are detailed in Supplementary Table S1. For synapse studies, nontransduced or transduced T cells ($1–2 \times 10^5$) were coincubated for 15 minutes with Raji cells labeled with 10 μmol/L 7-amino-4-chloromethylcoumarin (CMAC; cat. C2110, Life Technologies), at 1:1 E:T ratio, on poly-L-lysine (cat. P4832, Sigma-Aldrich)–coated coverslips, at 37°C, 5% CO_2. For CD19 localization studies, NT-T, CAR-T19, or STAb-T19 cells (1×10^5) were coincubated with CMAC-labeled NALM6 cells at 2:1 E:T ratio in U-bottom 96-well plates, and after 2 hours, cocultures were incubated on poly-L-lysine–coated coverslips at 37°C, 5% CO_2. Then, cells were fixed with 4% paraformaldehyde (cat. P6148, Sigma-Aldrich) and permeabilized with 0.1% Triton X100 (cat. 9036-19-5, Sigma-Aldrich) at room temperature, as previously described (17). For synapse studies, samples were stained with mouse anti-CD3ε supernatant (1/2 dilution; T3b clone; kindly provided by Dr. Francisco Sánchez-Madrid, Hospital Universitario de la Princesa, Madrid, Spain) and Phalloidin-647 (1/200 dilution; cat. 10656353, Fisher Scientific) for 1 hour at room temperature. For CD19 localization studies, samples were stained with anti-CD3ε (T3b clone), anti-CD19 supernatant (1/2 dilution; BU12 clone; kindly provided by Dr. Francisco Sánchez-Madrid), and anti-CD107a (BioLegend) antibodies. Cells were then washed 3 times for 5 minutes with TBS (20 mmol/L tris pH 7.4, 150 mmol/L NaCl) and incubated with goat anti-mouse-Ig Alexa Fluor 488 (catalog no. A11029, Life Technologies) for 30 minutes at room temperature. Finally, coverslips were washed and mounted with Mowiol (catalog no. 81381, Sigma-Aldrich). Confocal sections of fixed samples were acquired using an SP-8 laser scanning laser confocal microscopy (Leica Microsystems). For 3D reconstructions, z-stacks through the complete synapse were acquired every 0.3 μm. Actin clearance was estimated by the ratio:area of central region of the synapse depleted of actin/complete area of the synapse, including the actin ring, in 3D images. CD3 coalescence and cSMAC formation were assessed by visual inspection of 3D images. 3D reconstruction and image quantitation were performed with ImageJ freeware (NIH).

In vivo B-ALL xenograft models

Nine-week-old NOD.Cγ-Prkdcscid-IL2rgtm1Wjl/SzJ mice (NSG; The Jackson Laboratory) were infused intravenously (i.v.) with 1×10^6 $NALM6^{Luc}$ cells, and after 2 days received 5×10^6 NT-T, CAR-T19 (10% 19-CAR^+), or STAb-T19 (10% 19-$BiTE^+$) cells. Tumor growth was evaluated weekly by bioluminescence imaging as previously described (18). Briefly, 150 mg/kg of D-luciferin (catalog no. E1605, Promega) was administrated intraperitoneally in 200 μL of sterile PBS. Animals were imaged 10 minutes after D-luciferin injection using the Xenogen IVIS Lumina II imaging system (Caliper Life Sciences). The photon flux emitted by the luciferase-expressing cells was measured as an average radiance (photons/sec/cm_2/sr). Imaging analysis was performed using the Living Image Software 3.2 (Caliper Life Sciences). Tumor burden and T-cell persistence were analyzed by flow cytometry in PB, obtained by facial vein puncture, at day 19, and in spleen and BM samples after euthanization. Human CD19 relative gene expression in BM was analyzed by qRT-PCR. Briefly, total RNA was isolated with the RNeasy Micro Kit (catalog no. 74004, Qiagen) and cDNA was synthesized using NZY First-Strand cDNA Synthesis Kit (catalog no. MB125, Nzytech). qRT-PCR was performed with LightCycler 480 SYBR Green I Master Kit (catalog no. 04707516001, Roche Diagnostics) on a LightCycler 480 system (Roche Diagnostics). Each sample was analyzed in triplicate, and fold-expression changes were calculated with the equation $2^{-\Delta Ct}$. Human succinate dehydrogenase gene expression was used to normalize. The following primers, synthesized by Roche Diagnostics, were used:

F-hSDHA (5′-TGGGAACAAGAGGGCATCTG-3′)
R-hSDHA (5′-CCACCACTGCATCAAATTCATG-3′)
F-hCD19 (5′-agagatatgtgggtaatggag-3′)
R-hCD19 (5′-ttgccacggtgacaataatac-3′)

Body weight was monitored over time. Animals showing endpoint weight loss or clinical signs of leukemic disease or xenogenic graft-versus-host disease (xGVHD) were euthanized. For studies in a B-ALL PDX model, 6- to 12-week-old NSG mice were irradiated (2 Gy) and i.v. transplanted with 1×10^6 $CD19^+CD22^+CD10^+$ B-ALL blasts. Mice were i.v.-infused 3 weeks later with 3 or 5×10^6 NT, CAR-T19, or STAb-T19 cells (percentage of 19-CAR^+ or 19-$BiTE^+$ is indicated). Tumor burden was followed by bleeding every 1 or 2 weeks and BM extraction from tibial aspirates at different time points, cell staining with CD3-PerCP/CD10-PCy7/CD19-BV421/CD45-AmCyan/HLA-ABC-APC and subsequent flow cytometry analysis. Mice were euthanized when they had >5% blasts in PB or when they developed signs of xGVHD. Tumor burden and effector T-cell persistence were analyzed in BM, PB, and spleen by flow cytometry after staining cells with CD3-PerCP/CD10-PCy7/CD19-BV421/CD45-AmCyan/HLA-ABC-APC. *CD19* mRNA expression in BM was analyzed by qPCR, as described above.

Statistical analysis

Results of experiments are expressed as mean ± standard deviation (SD). Graphics and the statistical tests indicated in figure legends were done with Prism 6 (GraphPad Software).

Ethical issues

In vivo studies with the NALM6 cell line–derived xenograft model were carried out at CBM-SO in accordance with the guidelines of the Animal Experimentation Ethics Committee of the Spanish National Research Council. *In vivo* studies with the B-ALL PDX model were performed in the Barcelona Biomedical Research Park. All procedures were performed in compliance with the institutional animal care committee of the Barcelona Biomedical Research Park (DAAM7393).

Results

Engineered STAb-T19 cells efficiently secrete anti-CD19/CD3 BiTE and promote the formation of canonical immunologic synapses

This study was performed using engineered T cells expressing either a second-generation (CD8TM-4-1BB-CD3ζ) anti-CD19 CAR (13) or an anti-CD19/CD3 BiTE (referred to as 19-CAR or 19-BiTE, respectively), both using the clinically validated anti-CD19 A3B1 scFv (refs. 13, 16, 19; Supplementary Fig. S1). The 19-BiTE has a 6xHis-tag for immunodetection. Both constructs were cloned under the control of the EF1α promoter in both monocistronic and T2A-based bicistronic (19-BBζ-T2A-GFP and 19-BiTE-T2A-tdTo) lentiviral vectors (ref. 20; Supplementary Fig. S1). Gene transfer of 19-CAR and 19-BiTE vectors into primary human T cells was achieved with both lentiviral vector systems. The 19-BiTE was efficiently secreted by transduced primary human T cells (STAb-T19) with the expected molecular weight of 55 kDa (**Fig. 1A**). The secreted 19-BiTE specifically recognized plastic-immobilized human CD19 Fc chimeric protein (CD19-Fc; Supplementary Fig. S2A), and target cells expressing either cognate antigen (CD3 or CD19; Supplementary Fig. S2B). 19-BiTE intracellular expression and positive surface staining (decoration) of STAb-T19 cells was

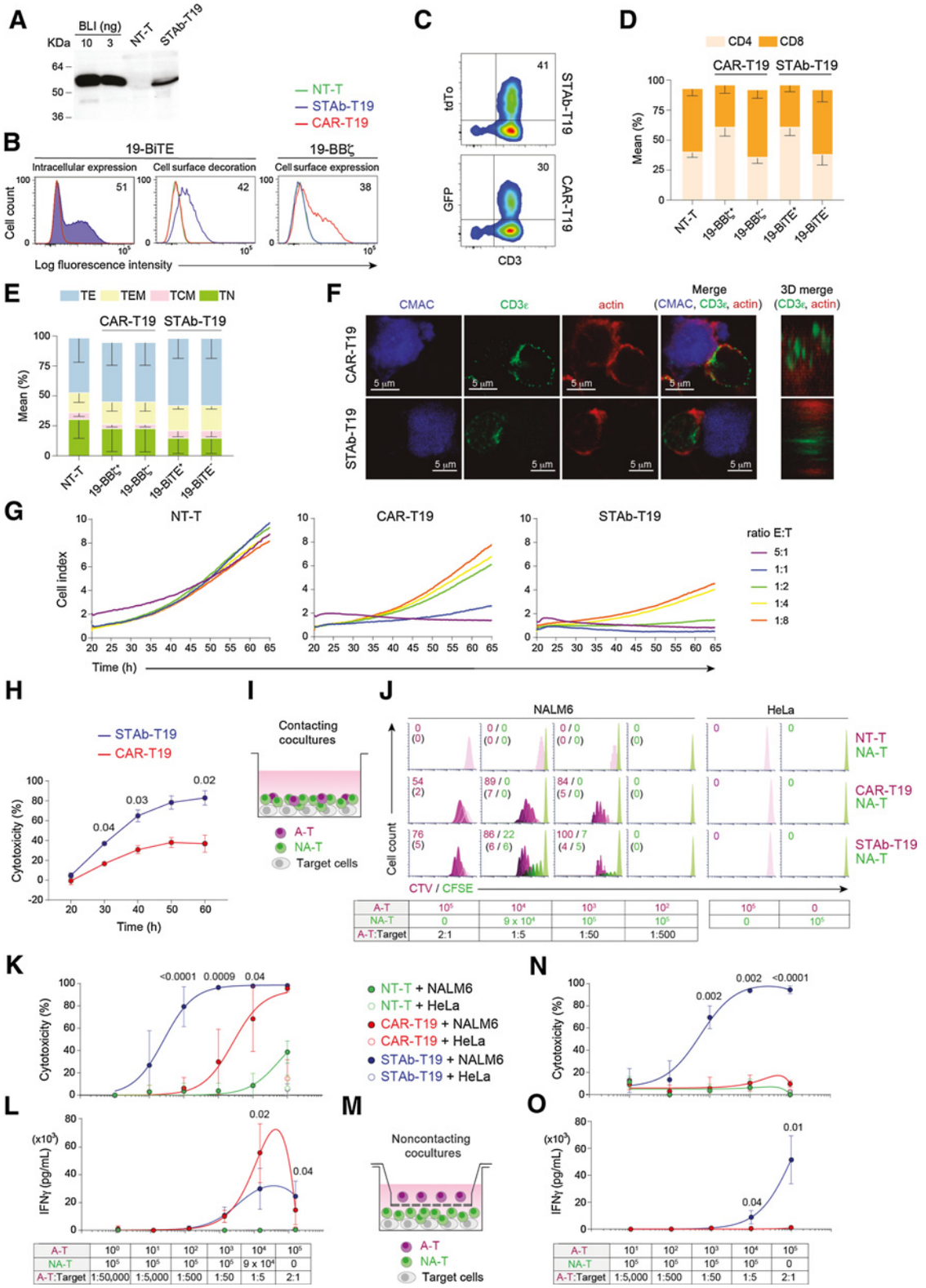
A
BLI (ng)
KDa 10 3
NT-T
STAb-T19
64
50
36
NT-T
STAb-T19
CAR-T19
B
19-BiTE
19-BBζ
Intracellular expression
Cell surface decoration
Cell surface expression
Cell count
51
42
38
Log fluorescence intensity
C
tdTo
GFP
CD3
STAb-T19
CAR-T19
41
30
D
CD4
CD8
CAR-T19
STAb-T19
Mean (%)
NT-T
19-BBζ*
19-BBζ-
19-BiTE*
19-BiTE-
E
TE
TEM
TCM
TN
CAR-T19
STAb-T19
Mean (%)
NT-T
19-BBζ*
19-BBζ-
19-BiTE*
19-BiTE-
F
CMAC
CD3ε
actin
Merge (CMAC, CD3ε, actin)
3D merge (CD3ε, actin)
CAR-T19
STAb-T19
5 μm
G
NT-T
CAR-T19
STAb-T19
Cell index
Time (h)
ratio E:T
5:1
1:1
1:2
1:4
1:8
H
STAb-T19
CAR-T19
Cytotoxicity (%)
0.02
0.03
0.04
Time (h)
I
Contacting cocultures
A-T
NA-T
Target cells
J
NALM6
HeLa
NT-T
NA-T
CAR-T19
NA-T
STAb-T19
NA-T
Cell count
CTV / CFSE
A-T 10⁵ 10⁴ 10³ 10² | 10⁵ 0
NA-T 0 9 x 10⁴ 10⁵ 10⁵ | 0 10⁵
A-T:Target 2:1 1:5 1:50 1:500
K
Cytotoxicity (%)
<0.0001
0.0009
0.04
NT-T + NALM6
NT-T + HeLa
CAR-T19 + NALM6
CAR-T19 + HeLa
STAb-T19 + NALM6
STAb-T19 + HeLa
L
IFNγ (pg/mL)
(x10³)
0.02
0.04
A-T 10⁰ 10¹ 10² 10³ 10⁴ 10⁵
NA-T 10⁵ 10⁵ 10⁵ 10⁵ 9 x 10⁴ 0
A-T:Target 1:50,000 1:5,000 1:500 1:50 1:5 2:1
M
Noncontacting cocultures
A-T
NA-T
Target cells
N
Cytotoxicity (%)
0.002
0.002
<0.0001
O
IFNγ (pg/mL)
(x10³)
0.01
0.04
A-T 10¹ 10² 10³ 10⁴ 10⁵
NA-T 10⁵ 10⁵ 10⁵ 10⁵ 0
A-T:Target 1:5,000 1:500 1:50 1:5 2:1

observed with an anti–His-tag mAb, indicating that secreted BiTEs bound to the CD3 complexes on the T-cell surface (**Fig. 1B**; Supplementary Fig. S2C and S2D). The percentage of 19-CAR$^+$ T cells was determined by labeling with a polyclonal Fab-targeting antibody (**Fig. 1B**; Supplementary Fig. S2E). Comparable transduction efficiencies were observed according to the percentage of tdTo$^+$ or GFP$^+$ cells (**Fig. 1C**; Supplementary Fig. S2F and S2G). Jurkat T cells were transduced at the same multiplicity of infection (MOI), albeit with more homogeneous expression profiles than primary T cells (Supplementary Fig. S2H). Lentivirus-transduced primary T cells that were 19-CAR$^+$ or 19-BiTE$^+$ showed a higher proportion of CD4$^+$ than CD8$^+$ T cells (**Fig. 1D**). The relative distribution of naïve, central memory, effector memory, and effector T-cell subsets was similar in nontransduced (NT)-T cells and in CAR-T19 and STAb-T19, with the most prevalent subset being effector T cells (**Fig. 1E**).

Following interaction with CD19$^+$ Raji cells, primary STAb-T19 cells organized a canonical immunologic synapse (IS), with normal filamentous (F)-actin–containing distal supramolecular activation cluster (dSMAC) and accumulation of CD3ε at the central SMAC (cSMAC; **Fig. 1F**; Supplementary Fig. S3A-S3E). In contrast, CAR-T19 cells formed a noncanonical IS with disperse clusters of CD3ε, and F-actin not properly cleared from the central area of interaction (**Fig. 1F**; Supplementary Fig. S3A–S3E). In an impedance-based real-time cytotoxicity assay, STAb-T19 cells were found to mediate rapid reduction of CD19$^+$ target cell viability (Supplementary Fig. S4A) at all E:T ratios, whereas CAR-T19 cells showed a lesser cytotoxic effect that required higher E:T ratios (**Fig. 1G**). When displayed as the percentage of cytotoxicity at several time points, STAb-T19 cells were significantly more effective than CAR-T19 cells (**Fig. 1H**). In contrast, CD19$^+$ cells cocultured with NT-T cells (**Fig. 1G**), or CD19$^-$ cells cocultured with NT-T, CAR-T19 or STAb-T19 cells (Supplementary Fig. S4C), displayed similar viability kinetics to those of target cells cultured alone (Supplementary Fig. S4B). Furthermore, analysis of CD107a staining showed higher degranulation activity in STAb-T19 cells compared with CAR-T19 cells following stimulation with CD19$^+$ targets (Supplementary Fig. S5).

STAb-T19 cells recruit bystander T cells and induce a more potent and rapid cytotoxic response than CAR-T19 cells

To assess STAb-T19 cell ability to recruit bystander T cells, we designed different *in vitro* coculture assays. NT or lentivirus-transduced activated T cells (A-T), or mixtures of A-T and freshly isolated T cells (nonactivated T cells, NA-T) from the same healthy donor were cocultured with CD19$^+$ or CD19$^-$ cells at a constant 2:1 T cell:target cell ratio (**Fig. 1I**). The A-T (NT-T, CAR-T19, or STAb-T19) were mixed with NA-T cells at different proportions (from 1/10 to 1/100,000) while keeping a constant total number of 1×10^5 effector T cells. When stimulated with NALM6 cells in a direct cell–cell contact context (**Fig. 1I**), the STAb-T19 cells proliferated efficiently and exhibited a higher percentage of dividing cells than CAR-T19 at the different A-T:target ratios (**Fig. 1J**). Importantly, STAb-T19 cells efficiently stimulated bystander NA-T cells to proliferate in the presence of NALM6 cells (**Fig. 1J**). This ability to recruit bystander NA-T cells allowed STAb-T19 cells to induce 100% lysis of tumor cells even at the 1:50 A-T:target ratio (**Fig. 1K**). Around 80% and 30% of specific target cell lysis persisted at 1:500 and 1:5,000 A-T:target ratios, respectively (**Fig. 1K**). The cytotoxic capacity of CAR-T19 cells rapidly declined as the A-T:target ratio decreased, from 60% lysis of NALM6 cells at a 1:5 A-T:target ratio to no apparent lysis at the 1:500 A-T:target ratio (**Fig. 1K**). In this context, the secretion of IFNγ by CAR-T19 cells was higher than in STAb-T19 cells (**Fig. 1L**). No significant proliferation or IFNγ secretion was observed when NA-T cells were mixed with NT-T cells and NALM6 cells (**Fig. 1I–L**); however, some degree of cytotoxicity was observed at the highest E:T ratio, attributable to allogeneic T-cell–activation against target cells (13). Transwell assays were used to further demonstrate that STAb-T19 cells were able to recruit bystander NA-T cells to CD19$^+$ cells. CD19$^+$ or CD19$^-$ target cells were plated with NA-T cells in the bottom well, and NT-T, CAR-T19, or STAb-T19 cells were plated in the insert well (**Fig. 1M**). Tumor cell killing (**Fig. 1N**) and IFNγ secretion (**Fig. 1O**) were totally dependent on the presence of STAb-T19 cells in the insert well, indicating that secreted 19-BiTEs effectively redirected the cytotoxicity of NA-T cells to CD19$^+$ targets. T cell lysis (70%) was induced at a STAb-T19:NA-T ratio of 1:50 and an overall E:T ratio of 2:1 in this transwell setup, demonstrating an efficient recruitment of bystander T cells by STAb-T19 cells (**Fig. 1N**).

STAb-T19 cells prevent leukemia escape *in vitro*

We next studied the ability of B-ALL cells to escape from immune control by coculturing CAR-T19 and STAb-T19 cells with NALM6 cells at low E:T ratios. STAb-T19 cells completely eliminated all leukemia cells, even at the 1:16 E:T ratio (**Fig. 2A**). By contrast,

Figure 1.

Comparative *in vitro* study of engineered STAb-T19 and CAR-T19 cells. **A,** Western blot detection of secreted 19-BiTE in the conditioned media from lentivirus-transduced human primary T cells (STAb-T19). Conditioned media from nontransduced T cells (NT-T) and media containing blinatumomab (BLI) were used as negative and positive controls, respectively. One representative experiment of three is shown. **B,** Representative analysis of intracellular and cell surface–bound 19-BiTE (decoration), and cell surface–expressed 19-CAR in NT-T and engineered CAR-T19 and STAb-T19 cells by flow cytometry. One representative experiment out of three independent experiments is shown. The numbers represent the percentage of cells staining positive for the indicated marker. **C,** Percentage of reporter protein expression in STAb-T19 cells (tdTo) and CAR-T19 cells (GFP). One representative transduction out of three performed is shown. **D** and **E,** Percentage of CD4$^+$ and CD8$^+$ T cells (**D**) and naïve (T_N), central memory (T_{CM}), effector memory (T_{EM}), and effector (T_E) T cells (**E**) among NT-T, CAR-T19, or STAb-T19 cells 7 days after transduction (means ± SD of three independent experiments are shown). **F,** Representative images of immunologic synapse (IS) assembly by primary CAR-T19 and STAb-T19 cells stimulated for 15 minutes with CMAC (blue)-labeled CD19$^+$ cells, stained for CD3ε and actin at the mature IS, with IS topology obtained from 3D reconstructions of regions of interest in confocal stacks. **G** and **H,** Real-time cell cytotoxicity assay with HEK-293^{CD19} target cells cocultured with NT-T, CAR-T19, or STAb-T19 cells at the indicated E:T ratios, and cell index values determined every 15 minutes for 65 hours using an impedance-based method (**G**) and percentage lysis normalized to NT-T cells (E:T ratio = 0.5:1; **H**), presented from one representative experiment performed in duplicate. **I,** Schematic representation of the direct contact coculture system used to study the ability of secreted 19-BiTE to induce bystander T-cell proliferation. **J,** Bystander T-cell proliferation after 5 days of coculture, with percentage of dividing cells and the number of cell divisions in parentheses. The total E:T ratio was constant (2:1), but the ratios A-T:target and A-T:NA-T varied as indicated. One representative experiment from three independent experiments is shown. **K,** Cytotoxicity induced by varying numbers of A-T and NA-T cells from the same donor cocultured with NALM6^{Luc} or HeLa^{Luc} target cells for 48 hours, maintaining a constant 2:1 E:T ratio, measured by adding D-luciferin to detect bioluminescence. Data are shown as mean ± SD from four replicates. Significance was calculated by an unpaired Student *t* test. **L,** IFNγ secretion was determined by ELISA. Data are mean ± SD of three independent experiments. Significance was calculated by an unpaired Student *t* test. **M,** Cocultures were performed in a noncontacting transwell system; NALM6^{Luc} or HeLa^{Luc} target cells and NA-T cells were plated in the bottom well and A-T cells (NT-T, CAR-T19, or STAb-T19) in the insert well. **N** and **O,** After 48 hours, the percentage of cytotoxicity (**N**) was determined by luciferase assay, and IFNγ secretion (**O**) was determined by ELISA. Data are shown as mean ± SD from three and four replicates, respectively. Significance was calculated by an unpaired Student *t* test.

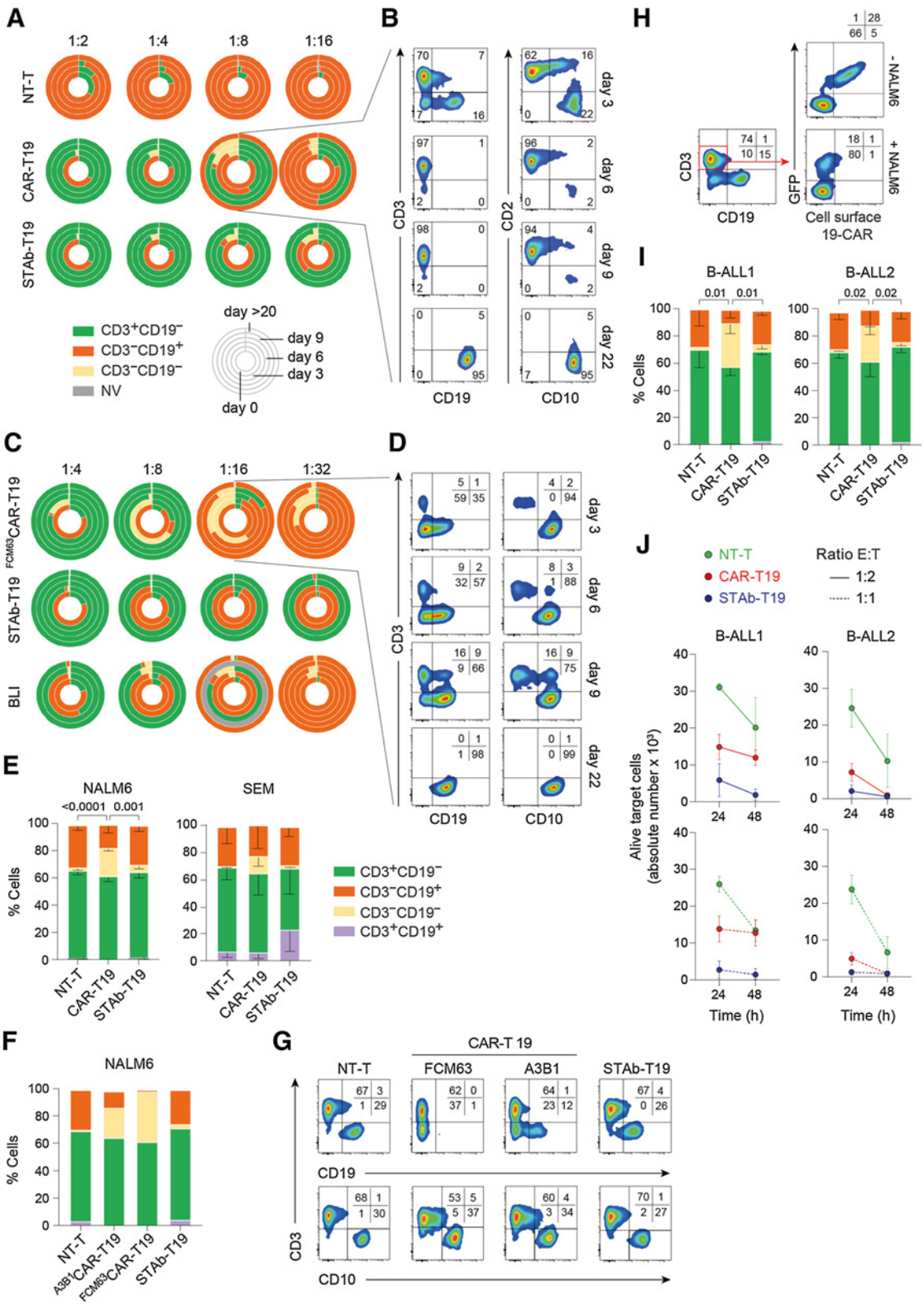
A
1:2
1:4
1:8
1:16
NT-T
CAR-T19
STAb-T19
CD3+CD19−
CD3−CD19+
CD3−CD19−
NV
day >20
day 9
day 6
day 3
day 0
B
CD3
CD19
CD2
CD10
day 3
day 6
day 9
day 22
C
1:4
1:8
1:16
1:32
FCM63CAR-T19
STAb-T19
BLI
D
CD3
CD19
CD10
day 3
day 6
day 9
day 22
E
NALM6
SEM
<0.0001
0.001
% Cells
NT-T
CAR-T19
STAb-T19
CD3+CD19−
CD3−CD19+
CD3−CD19−
CD3+CD19+
F
NALM6
% Cells
NT-T
A3B1CAR-T19
FCM63CAR-T19
STAb-T19
G
CAR-T 19
NT-T
FCM63
A3B1
STAb-T19
CD19
CD3
CD10
H
CD3
CD19
GFP
Cell surface 19-CAR
- NALM6
+ NALM6
I
B-ALL1
B-ALL2
0.01
0.02
% Cells
NT-T
CAR-T19
STAb-T19
J
NT-T
CAR-T19
STAb-T19
Ratio E:T
1:2
1:1
B-ALL1
B-ALL2
Alive target cells (absolute number x 10³)
Time (h)
24
48

CAR-T19 cells did not eliminate $CD19^+$ cells at E:T ratios of 1:8 or lower, where leukemia cells persisted with a partial downmodulation of CD19 (**Fig. 2A** and **B**; Supplementary Fig. S6). In some cases, NALM6 cells had almost completely lost surface expression of CD19 by day 6 (which continued to day 9; **Fig. 2B**; Supplementary Fig. S6). Preincubation of NALM6 cells with A3B1 scFv only partially blocked the binding of the J3.119 antibody, suggesting that they recognize nonoverlapping epitopes on CD19 (Supplementary Fig. S7). Furthermore, CD10 remained unchanged in NALM6 cells (**Fig. 2B**). Thereafter, leukemia cells progressed and recovered surface expression of CD19, suggesting that antigen downmodulation functions as an escape mechanism against CAR-T19 pressure (**Fig. 2A** and **B**; Supplementary Fig. S6). The CD19 downmodulation effect was even more pronounced when NALM6 cells were cocultured with CAR-T19 cells bearing an anti-CD19 FMC63 scFv-based 4-1BBζ CAR (^{FMC63}CAR-T19; ref. 13), which also failed to control tumor cell growth at the lowest rates analyzed (1:16 and 1:32; **Fig. 2C** and **D**). Two different 19-BiTEs, either *in situ*–secreted A3B1 BiTE or exogenously added HD37 BiTE (a.k.a. blinatumomab, BLI), were not associated with a loss of CD19 expression (**Fig. 2C**). Importantly, STAb-T19 cells were more effective than the addition of BLI to the coculture, as *in situ*–secreted A3B1 BiTE eliminated leukemic cells even at a 1:32 ratio, whereas NALM6 cells persisted after exogenous administration of BLI at the two lower ratios (**Fig. 2C**). This is likely explained by the fact that STAb-T19 cells continuously secrete and display a stable quantity of 19-BiTE decoration, whereas exogenously administered BLI is cleared from the cell surface in a relatively short period of time (Supplementary Fig. S8).

Next, CAR-T19 and STAb-T19 cells were cocultured at 2:1 E:T ratio with two B-ALL cell lines (NALM6 and SEM) and two primary B-ALL cells (B-ALL1 and B-ALL2) for 2 hours. Both B-ALL cell lines showed a rapid decrease of surface CD19 expression after coculture with CAR-T19 cells (**Fig. 2E**). CD19 reduction was more intense when NALM6 cells were cocultured with ^{FMC63}CAR-T19 cells, whereas CD10 expression was unchanged (**Fig. 2F** and **G**). Concomitantly, the 19-CAR was profoundly downmodulated from CAR-T19 cell surface after encountering $CD19^+$ cells, whereas the expression of CD3 was unaffected (**Fig. 2H**). A significant CD19 downmodulation was also observed in cocultures of primary B-ALL cells with CAR-T19 cells (**Fig. 2I**). In contrast, CD19 was not lost after coculture of STAb-T19 cells with either B-ALL cell lines or primary B-ALL cells (**Fig. 2E–I**). We next assessed the cytotoxic activity of CAR-T19 and STAb-T19 cells against primary B-ALL cells. STAb-T19 cells were able to eliminate nearly 100% of the primary B-ALL blasts after 24 hours, whereas CAR-T19 cells exerted a weaker cytotoxic effect (B-ALL1) or required 48 hours to kill 100% of tumor cells (B-ALL2; **Fig. 2J**; Supplementary Table S2).

Leukemia escape is associated with rapid and drastic CAR-mediated CD19 downmodulation

To more carefully study the mechanism of leukemia escape, NALM6 cells were cocultured for 2 hours at a 1:1 E:T ratio with lentivirus-transduced Jurkat T cells homogeneously expressing high amounts of A3B1-based 19-CAR (J-CAR-T19) or 19-BITE (J-STAb-T19; Supplementary Fig. S2H). Although NALM6 cells showed a rapid and intense downmodulation of CD19 (**Fig. 3A**), the 19-CAR disappeared completely from the J-CAR-T19 cell surface (**Fig. 3B**). Membrane CD19 was not reduced in NALM6 after coculture with J-STAb-T19 cells (**Fig. 3A**). In order to locate CD19, NALM6 cells were cocultured with effector T cells, costained for CD19 and the lysosomal marker LAMP1, and analyzed by confocal microscopy. In cocultures with J-CAR-T19 cells, a reduction of cell-surface CD19 (**Fig. 3C**) and a clear colocalization of intracellular CD19 in lysosomes (**Fig. 3C** and **D**) was observed. The presence of CD19 in lysosomes was much lower in target cells cocultured with either J-STAb-19 or nontransduced Jurkat cells (**Fig. 3C** and **D**).

STAb-T19 cells are as effective as CAR-T19 cells in short-term *in vivo* models

To study the *in vivo* antitumor effects of CAR-T19 and STAb-T19 cells in a xenograft model, 1×10^6 $NALM6^{Luc}$ cells were injected intravenously (i.v.) in NSG mice, followed 2 days later by 5×10^6 primary T cells (NT-T, CAR-T19, or STAb-T19), where 19-CAR^+ or 19-$BITE^+$ T cells accounted for 10% of the infused T cells (5×10^5; **Fig. 4A**). Mice receiving NT-T cells were sacrificed within the first three weeks due to leukemia progression, whereas CAR-T19– and STAb-T19–treated mice effectively controlled $NALM6^{Luc}$ cells (**Fig. 4B** and **C**).

Notably, in contrast to STAb-T19–treated mice, 2 of the 6 mice that received CAR-T19 cells developed early cases of severe xenogeneic graft-versus-host disease (xGvHD) and had to be euthanized before week 5 (**Fig. 4B** and **D**). Flow cytometry analysis confirmed the bioluminescence imaging data, with an absence of leukemia cells in peripheral blood (PB), BM and spleen in mice treated with either CAR-T19 or STAb-T19 cells (**Fig. 4E**). qRT-PCR analysis confirmed the absence of CD19 transcripts in BM from both groups (**Fig. 4F**). Regarding T-cell persistence, we found a marked expansion of $CD3^+$ cells in PB, spleen, and BM in both groups (**Fig. 4G**), which could be a consequence of the xGvHD. In a more clinically relevant PDX model (**Fig. 4H**), NSG mice were i.v.-injected with 1×10^6 primary B-ALL cells homogeneously expressing CD19, CD22, and CD10 (**Fig. 4I**), followed 3 weeks later by i.v. infusion of 5×10^6 T cells (**Fig. 4H**), where 19-CAR^+ or 19-$BITE^+$ T cells comprised 10% of the infused T cells. An aggressive leukemia progression was observed in both BM (96.7% ± 0.5% on week 4) and PB (2.2 ± 1.3% and

Figure 2.

Leukemia escape from immune pressure. **A** and **B,** NALM6 cells were cocultured with NT-T, CAR-T19, or STAb-T19 cells at the indicated E:T ratios, and the relative percentage of $CD3^+CD19^-$, $CD3^-CD19^+$, and $CD3^-CD19^-$ cells were measured by FACS. **A,** Results are shown as the mean of three independent experiments. **B,** Representative FACS dot plots of the CAR-T19 1:8 E:T ratio sample. Gray, nonviable (NV), in which number of cells in the culture was <500. **C** and **D,** NALM6 coculture as in **A–B**, with CAR-T19 bearing the anti-CD19 FMC63 scFv (^{FMC63}CAR-T19), STAb-T19, or with NT-T cells in the presence of 100 ng/mL blinatumomab (BLI). One representative experiment out of two is shown. Dot plots (**D**) showing the cell populations cocultured at a 1:16 E:T ratio. **E,** The percentages of $CD3^+CD19^-$, $CD3^-CD19^+$, and $CD3^-CD19^-$ and $CD3^+CD19^+$ NALM6 or SEM cell lines after 2 hours of coculture with A-T cells at a 2:1 E:T ratio. The results are means of 3 ± SD similar experiments. **F** and **G,** The percentages of $CD3^+CD19^-$, $CD3^-CD19^+$, $CD3^-CD19^-$, and $CD3^+CD19^+$ NALM6 cells after coculture with NT-T cells, CAR-T19 cells bearing the anti-CD19 FMC63 scFv (^{FMC63}CAR-T19) or the anti-CD19 A3B1 (^{A3B1}CAR-T19), or STAb-T19 cells. **H,** Representative dot plots showing the downmodulation of 19-CAR in ^{A3B1}CAR-T19 cells after 2 hours of coculture with NALM6 cells. One representative experiment out of three independent experiments is shown. **I,** The percentage of $CD3^+CD19^-$, $CD3^-CD19^+$, $CD3^-CD19^-$, and $CD3^+CD19^+$ primary human B-ALL cells from two different patients (B-ALL1 and B-ALL2, >90% of $CD19^+$ B-ALL blasts) after coculture with primary A-T cells at a 2:1 E:T ratio. The results are means ± SD of 3 similar experiments. **J,** The number of alive ($7AAD^-$) target B-ALL1 and B-ALL2 cells determined after 24- and 48-hour coculture with primary NT-T, CAR-T19, or STAb-T19 cells at 1:2 and 1:1 E:T ratios. Results are shown as mean ± SD from 3 experiments. Significance was calculated by an unpaired Student *t* test.

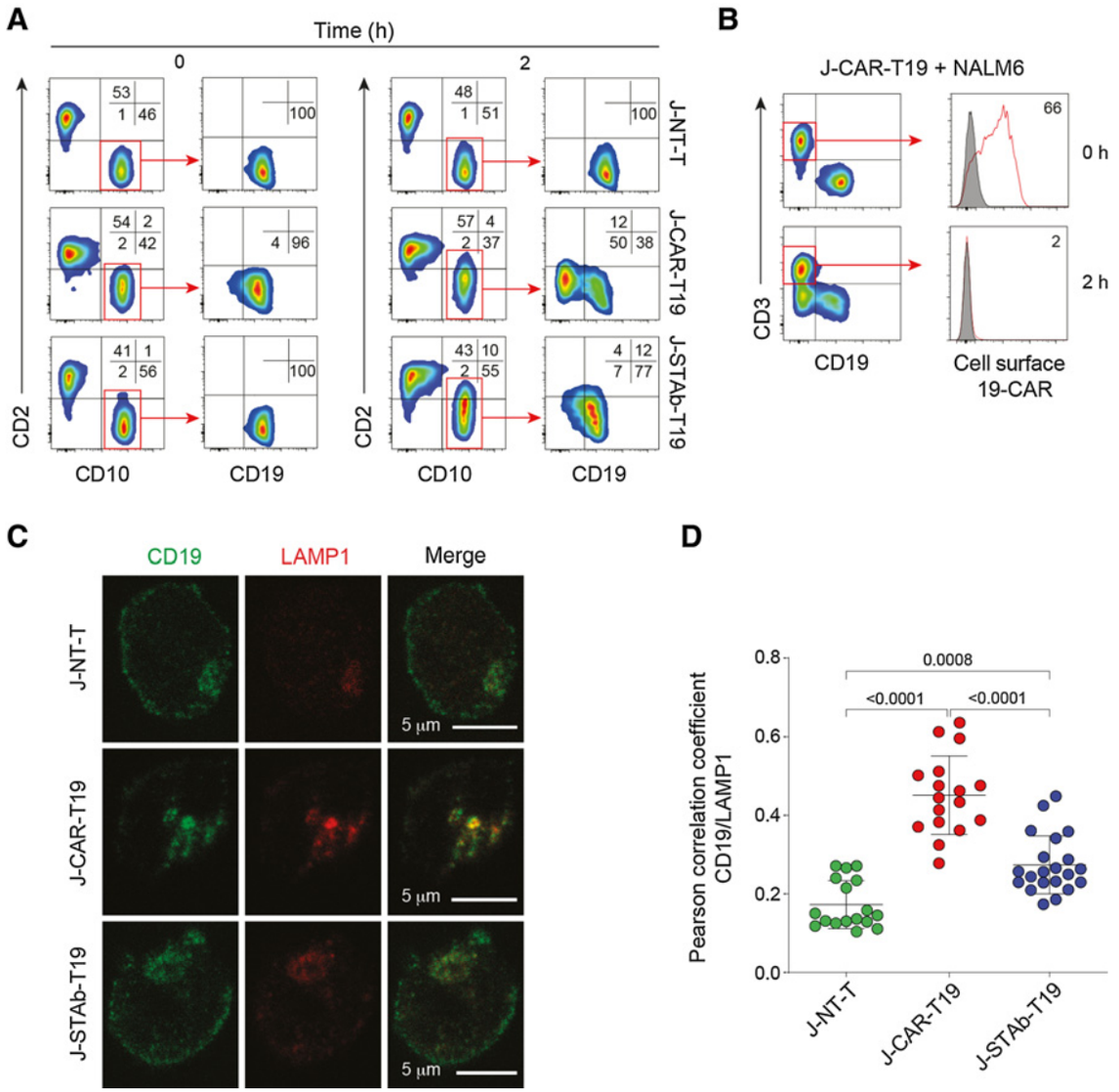

Figure 3.

CAR-T19 cells induced CD19 downmodulation and degradation. NALM6 cells were cocultured for 2 hours at a 1:1 E:T ratio with nontransduced Jurkat cells (J-NT), J-CAR-T19, or J-STAb-T19 cells. **A,** Representative dot plots showing CD2, CD19, and CD10 expression. **B,** Analysis of 19-CAR expression. **C,** Representative images of CD19 and LAMP1 cellular localization in NALM6 cells cocultured with J-NT-T, J-CAR-T19, or J-STAb-T19 cells. **D,** Pearson coefficients' for CD19 and LAMP1 colocalization assessment in NALM6 cells in the indicated cocultures. Dots represent the analyzed cells in one experiment representative of two performed. Mean ± SD values are shown. The *P* values were calculated with one-way ANOVA with Tukey multiple comparison tests.

12.1% ± 11.6%, on weeks 2 and 4, respectively) in NT-T cell–treated mice (**Fig. 4J** and **K**), that were euthanized 4 weeks after T-cell infusion due to the severity of the disease. In contrast, mice treated with CAR-T19 and STAb-T19 cells effectively controlled B-ALL growth for 8 weeks, when the mice were euthanized because of xGvHD (**Fig. 4J** and **K**). To exclude the presence of $CD19^-$ blasts, CD10 expression was analyzed by flow cytometry, and no $CD19^-CD10^+$ cells were detected in BM from CAR-T19– and STAb-T19–treated mice (**Fig. 4L**). T cells expanded progressively in PB, BM, and spleen, especially in the CAR-T19 group (**Fig. 4M**). These studies clearly showed that STAb-T19 cells are as effective as CAR-T19 cells in short-term *in vivo* models.

STAb-T19 cells prevent the leukemia relapse in long-term *in vivo* models

To test whether STAb-T19 cells can prevent escape *in vivo*, as observed *in vitro*, we modeled leukemia relapse by infusing lower doses of T cells to delay the onset of xGVHD and extend the observational window. NSG mice were i.v.-infused with 1×10^6 primary B-ALL cells from the same patient (**Fig. 4H** and **I**), followed 3 weeks later by i.v. infusion of 3×10^6 T cells [NT-T, CAR-T19 (5×10^5 19-CAR^+) or STAb-T19 (5×10^5 19-$BiTE^+$); **Fig. 5**A]. NT-T–treated mice rapidly developed leukemia, as shown by the increase in the percentage of blasts in PB early during week 2 and were sacrificed at week 5 (**Fig. 5B**). Both CAR-T19 and STAb-T19 groups initially controlled disease

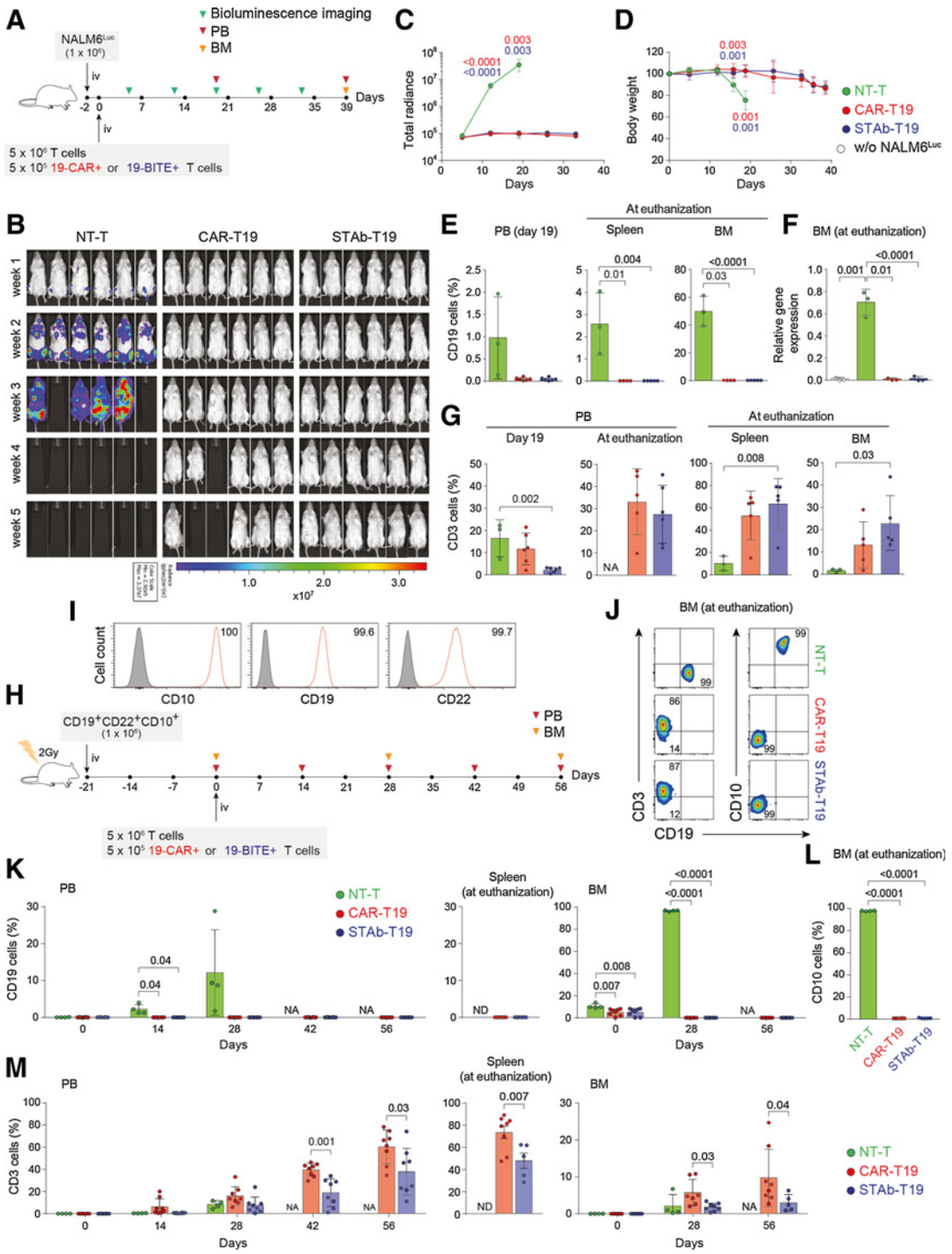

Figure 4.

In vivo antitumor efficacy of STAb-T19 cells. **A,** Timeline of cell line–derived xenograft murine model of NSG mice ($n = 6$/group) receiving i.v. NALM6^{Luc} cells followed by NT-T, CAR-T19, or STAb-T19 cells. **B,** Bioluminescence images showing disease progression. **C,** Total radiance quantification at the indicated time points. **D,** Change in body weight over time. **E,** Detection by FACS of B-ALL cells (CD19$^+$) cells in PB at day 19, and in spleen and BM at euthanization. **F,** Relative mRNA expression of *CD19* in BM at euthanization. **G,** T-cell (CD3$^+$) persistence in PB at days 19 and 39, and in spleen and BM at euthanization. Data are shown as mean ± SD. **H,** Timeline of PDX murine model of NSG mice receiving i.v. CD19$^+$ CD22$^+$ CD10$^+$ B-ALL blasts followed NT-T ($n = 4$), CAR-T19 ($n = 8$), or STAb-T19 ($n = 8$) cells. **I,** CD10, CD19, and CD22 expression in primary human B-ALL cells with the percentage of positive cells. **J,** Representative dot plots showing human T cells and B-ALL cells in BM of mice at day 56 after infusion. **K,** Percentage of CD19$^+$ leukemic cells in PB, spleen, and BM at indicated time points. **L,** Percentage of CD10$^+$ leukemic cells in BM at euthanization. **M,** Human T-cell persistence over time in PB, spleen, and BM at the indicated time points. Data are shown as mean ± SD; each dot represents an independent mouse. Significance was calculated by an unpaired Student *t* test. NA, not applicable; ND, not determined.

progression (**Fig. 5B**). However, blasts in PB of CAR-T19–treated mice gradually increased from week 4, and mice were euthanized when they reached 5% CD19$^+$ blasts in PB, whereas no blasts were detected in STAb-T19–treated mice by week 15 (**Fig. 5B**). Accordingly, analyses of spleen and BM showed complete leukemia control in STAb-T19–treated mice, whereas blasts were found in CAR-T19–treated mice (**Fig. 5C**). qRT-PCR confirmed the absence of CD19 transcripts in BM from STAb-T19–treated mice (**Fig. 5D**). The presence of CD19-negative blasts in BM was excluded by flow cytometry analysis of CD10 expression (**Fig. 5E**). Regarding T-cell expansion and persistence, percentages of CD3$^+$ cells in PB were lower than those observed in the groups that received 5 × 10^6 T cells (**Figs. 4M**; **5F** and **G**), although CAR-T19 cells (CD3$^+$GFP$^+$) and STAb-T19 cells (CD3$^+$tdTo$^+$) at week 2 comprised nearly 10% of the peripheral T cells (**Fig. 5H**). Consistent with these antileukemic results and absence of xGvHD, a very significant disease-free and overall survival benefit was observed for the mice that had been treated with STAb-T19 cells ($P = 0.005$; **Fig. 5I**).

Discussion

In this study, we demonstrate that engineered T cells expressing soluble anti-CD19/CD3 BiTEs are more effective than engineered CAR T cells expressing a membrane-anchored second-generation anti-CD19 CAR at inducing specific cytotoxicity, preventing tumor escape *in vitro*, and leukemia relapse *in vivo*. STAb-T19 cells redirect bystander T cells efficiently, leading to a more rapid and effective cytotoxic activity, even at very low E:T ratios. This demonstrates that *in situ*–secreted anti-CD19/CD3 BiTEs efficiently decorate CD3 on the surface of bystander T cells, converting them into efficient leukemia killers. Notably, unlike CAR-T19 cells, STAb-T19 cells are able to achieve a high cytotoxic effect at E:T ratios in which IFNγ secretion is low. This could imply that an effective treatment with STAb-T19 cells might require lower doses than those used with CAR-T19 cells and could be of particular relevance in such cases where it is not possible to generate an adequate number of CAR T cells due to the lymphopenic status of many multitreated patients or due to manufacturing problems (21). Therefore, a reduction in

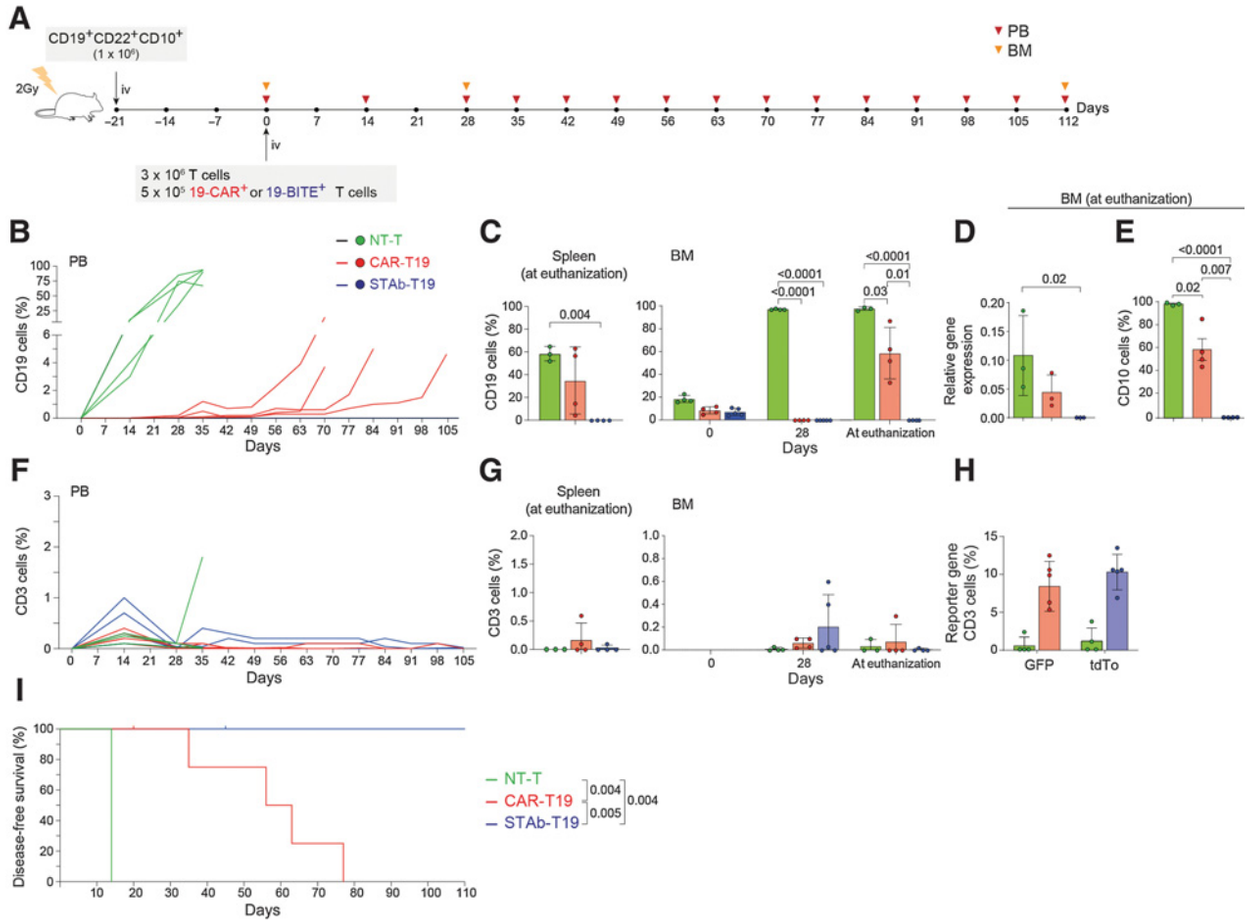

Figure 5.

STAb-T19 cells, but not CAR-T19, prevent relapse in a PDX murine model. **A,** Timeline of NSG mice transplanted with human primary CD19$^+$ CD22$^+$ CD10$^+$ B-ALL blasts followed by NT-T ($n = 4$), CAR-T19 ($n = 5$), or STAb-T19 ($n = 5$) cells. **B,** Percentage of B-ALL cells (CD19$^+$) in PB over time; each line represents an independent mouse. **C,** Percentage of human B-ALL cells in spleens and BM of NT-T, CAR-T19, and STAb-T19–treated mice at the indicated time points post-infusion. **D,** Relative mRNA expression of *CD19* in BM at euthanization, and (**E**) percentage of CD10$^+$ leukemic cells in BM at euthanization. **F,** Human T-cell (CD3$^+$) persistence over time in PB of each individual mouse. **G,** Percentage of human T cells (CD3$^+$) in spleen and BM at the indicated time points, and (**H**) percentage of human CD3$^+$ cells expressing reporter genes (GFP or tdTo). Data are shown as mean ± SD; each dot represents an independent mouse. Significance was calculated by an unpaired Student *t* test. **I,** Disease-free survival curve according to the percentage of CD19$^+$ B-ALL cells in PB. Significance was calculated by a log-rank test.

the therapeutically effective cell number may increase the number of patients who would benefit from STAb T-cell therapy, and significantly reduce the cost of the treatment. In addition, disease progression during the manufacturing period may, in some circumstances, preclude CAR T-based therapies (21), in which case the requirement for a lower number of cells and the accordingly shortened manufacturing time would be advantageous.

STAb-T19 cells, contrary to CAR-T19 cells, prevent *in vitro* tumor escape even at 1:32 E:T ratio. Leukemia escape is associated with rapid and drastic CAR-mediated CD19 downmodulation, alongside an intense loss of T-cell surface CAR. It has been reported that the density of the targeted antigen plays an important role in the modulation of CAR T cell–activation, which occurs only if a threshold density is reached (22). Therefore, the partial or complete loss of CD19 could explain the reduced cytotoxic activity of CAR-T19 cells. Importantly, this CAR-mediated CD19 downmodulation is also observed in engineered T cells expressing a second-generation CAR containing an scFv derived from the anti-CD19 clone FMC63, which has been used to generate the four FDA-approved anti-CD19 CAR T therapies (2). Furthermore, our data indicate that the rapid CAR-mediated internalization is associated with lysosome-mediated CD19 degradation. This leads to the emergence of a subpopulation of leukemic cells that transiently decrease CD19 expression and evade the immune response of CAR-T19 cells. Subsequently, when the CAR-mediated selective pressure is reduced or disappears, leukemia cells progress and recover CD19 expression. The rate of CD19 internalization upon binding to soluble anti-CD19 antibodies varies considerably (23, 24) and, in fact, has been shown that only a small fraction of an FMC63 scFv-based monovalent molecule bound to the surface is internalized (25). This suggests that membrane anchoring of the anti-CD19 scFv through the CAR is instrumental to induce CD19 internalization and could explain why we did not observe internalization following BiTE-mediated interaction. This phenomenon of CD19 downmodulation after CAR-T19 cell interaction, which has not been previously characterized, may have a major impact *in vivo*. Although both strategies show similar efficacy in short-term (40–60 days) mouse models, there is a drastic difference between the two CD19-targeted therapies in a long-term (over 100 days) PDX mouse model. In the long-term mouse model, STAb-T19 cells efficiently eradicated leukemia cells, whereas leukemia relapsed after CAR-T19 therapy. Most *in vivo* models used to study the efficacy of CAR T therapies in which complete remission is achieved are conducted with short- to intermediate-length windows of observation (13, 26, 27), which may lead to an underestimation of the risk of relapse after CAR-T19–based treatment.

In addition to CD19, CARs also undergo a rapid downmodulation after antigen engagement. Indeed, ligand-induced downmodulation is a common feature of antigen receptors such as TCR (28). CAR downmodulation has been reported to occur due to ubiquitination and lysosomal degradation (29) and leads to attenuation of the tumor killing ability of CAR T cells (29–31). In contrast, we did not observe such a drastic reduction of CD3 expression after BiTE-mediated interactions. Although the CAR- and BiTE-mediated T-cell redirection strategies are conceptually similar, they are very distinct in their implementation. CARs are artificial type I transmembrane proteins with variable modular architecture, which directly interacts with CD19, whereas soluble Fc-free BiTEs establish bridges between two type I transmembrane proteins, CD19 and the CD3ε subunit of the TCR/CD3 complex (5). Moreover, our findings support previous studies showing that, whereas CAR-T19 cells form noncanonical disorganized ISs (32–34), anti-CD19/CD3 BiTEs induce the formation of canonical ISs (35, 36), which promote efficient degranulation and prevent the CD19 downmodulation and degradation observed in CAR-mediated interactions. In summary, the absence of CD19 downmodulation in the STAb-T19 strategy, coupled with the continued secretion of BiTEs, allows a rapid recruitment of the endogenous T-cell pool, resulting in a fast and efficient elimination of cancer cells, which may prevent the leukemia relapse that is frequently associated with CAR-T19 therapies. Further studies are needed to fully evaluate the therapeutic capacity and toxicity profile of STAb-T19 cells in a clinical setting.

Authors' Disclosures

S. Guedan reports grants from the Spanish Ministry of Science and Innovation during the conduct of the study; grants from Spanish Ministry of Science and Innovation, Innovative Medicines Initiative 2, La Caixa, and Asociación Española contra el Cancer outside the submitted work; and she has received research funding from Gilead and Roche and personal honoraria from Gilead, Novartis, and Bristol-Myers Squibb. M. Juan reports a patent for EP3865513A1 pending. P. Menéndez reports grants from Onechain ImmunoTx during the conduct of the study and is the founder of Onechain Immnunotherapeutics, a spin-off company from the Josep Carreras Leukemia Research Institute. L. Álvarez-Vallina reports grants from CRIS Cancer Foundation, Carlos III Health Institute, Spanish Association Against Cancer, and Spanish Ministry of Science and Innovation during the conduct of the study; and cofounder of Leadartis, a spin-off focused on unrelated interest. No disclosures were reported by the other authors.

Authors' Contributions

B. Blanco: Conceptualization, resources, supervision, funding acquisition, investigation, methodology, writing–original draft, writing–review and editing. **A. Ramírez-Fernández:** Investigation, methodology, writing–original draft. **C. Bueno:** Resources, supervision, funding acquisition, investigation, methodology, writing–review and editing. **L. Argemí-Muntadas:** Investigation, methodology, writing–review and editing. **P. Fuentes:** Resources, investigation, methodology, writing–review and editing. **Ó. Aguilar-Sopeña:** Investigation and methodology. **F. Gutierrez-Agüera:** Validation, investigation, and methodology. **S.R. Zanetti:** Investigation, methodology, writing–review and editing. **A. Tapia-Galisteo:** Investigation and methodology. **L. Díez-Alonso:** Investigation and methodology. **A. Segura-Tudela:** Investigation and methodology. **M. Castellà:** Investigation and methodology. **B. Marzal:** Investigation and methodology. **S. Betriu:** Investigation and methodology. **S.L. Harwood:** Investigation, methodology, writing–review and editing. **M. Compte:** Investigation and methodology. **S. Lykkemark:** Investigation and methodology. **A. Erce-Llamazares:** Investigation and methodology. **L. Rubio-Pérez:** Investigation and methodology. **A. Jiménez-Reinoso:** Investigation and visualization. **C. Domínguez-Alonso:** Investigation and methodology. **M. Neves:** Investigation and methodology. **P. Morales:** Investigation and methodology. **E. Paz-Artal:** Investigation and methodology. **S. Guedan:** Investigation and methodology. **L. Sanz:** Funding acquisition, investigation, methodology, writing–review and editing. **M.L. Toribio:** Resources, funding acquisition, methodology, writing–review and editing. **P. Roda-Navarro:** Resources, funding acquisition, methodology, writing–review and editing. **M. Juan:** Resources, funding acquisition, investigation, methodology, writing–review and editing. **P. Menéndez:** Resources, supervision, funding acquisition, methodology, writing–review and editing. **L. Álvarez-Vallina:** Conceptualization, resources, formal analysis, supervision, funding acquisition, validation, investigation, writing–original draft, writing–review and editing.

Acknowledgments

We thank R. Vilella for generating and providing the A3B1 antibody, F. Sánchez-Madrid for reagents, and the staff of the fluorescence microscopy facility of the Complutense University of Madrid for assistance with the confocal microscopy. We thank CRIS Cancer Foundation, CERCA/Generalitat de Catalunya, and Fundació Josep Carreras-Obra Social la Caixa for core support. Financial support for this work was obtained from the European Research Council (CoG-2014-646903, PoC-2018-811220, to P. Menéndez); the Spanish Ministry of Science and Innovation (PID2019-105623RB-I00, to M.L. Toribio; SAF2016-75656-P and RTC-2017-5944-1, to P. Roda-Navarro; SAF-2019-108160-R, to

P. Menéndez; and SAF2017-89437-P, PID2020-117323RB-100, and PDC2021-121711-100, to L. Álvarez-Vallina), partially supported by the European Regional Development Fund (ERDF); the Carlos III Health Institute (ISCIII, PI20/01030, to B. Blanco; PI20/00822 to C. Bueno; PI16/00357 and PI19/00132 to L. Sanz; PICI14/122, PI13/676, PIE13/33, and PI18/775, to M. Juan; DTS20/00089, to L. Álvarez-Vallina), partially supported by the ERDF; the Obra Social La Caixa (LCF/PR/HR19/52160011, to P. Menéndez), CatSalut, Fundació La Caixa (CP042702, to M. Juan); the Spanish Association Against Cancer (AECC CICPF18030TORI, to M.L. Toribio; AECC 19084, to L. Álvarez-Vallina); Fundación Uno Entre Cien Mil, and Fundación Ramón Areces to M.L. Toribio; and the CRIS Cancer Foundation (FCRIS-IFI-2018 and FCRIS-IFI-2020, to L. Álvarez-Vallina). ISCIII-RICORS is supported within the Next Generation EU program (Plan de Recuperación, Transformación y Resiliencia). S. Guedan has received funding from the Spanish Ministry of Science and Innovation under a Ramon y Cajal grant (RYC2018-024442-I). A. Tapia-Galisteo was supported by predoctoral fellowship from Comunidad Autónoma de Madrid (PEJD-2018- PRE/BMD-8314). L. Díez-Alonso was supported by a Rio Hortega fellowship from the ISCIII (CM20/00004). L. Rubio-Pérez was supported by a predoctoral fellowship from the Immunology Chair, Universidad Francisco de Vitoria/Merck. C. Domínguez-Alonso was supported by a predoctoral fellowship from the Spanish Ministry of Science and Innovation (PRE2018-083445). M. Neves was supported by a grant from Portuguese Foundation for Science and Technology (SFRH/BD/136574/2018).

The costs of publication of this article were defrayed in part by the payment of page charges. This article must therefore be hereby marked *advertisement* in accordance with 18 U.S.C. Section 1734 solely to indicate this fact.

Received October 7, 2021; revised December 6, 2021; accepted February 9, 2022; published first February 14, 2022.

References

1. Blanco B, Compte M, Lykkemark S, Sanz L, Alvarez-Vallina LT. Cell-redirecting strategies to 'STAb' tumors: beyond CARs and bispecific antibodies. Trends Immunol 2019;40:243–57.
2. Frigault MJ, Maus MV. State of the art in CAR T cell therapy for CD19+ B cell malignancies. J Clin Invest 2020;130:1586–94.
3. Romero D. Haematological cancer: blinatumomab facilitates complete responses. Nat Rev Clin Oncol 2018;15:200.
4. Xu X, Sun Q, Liang X, Chen Z, Zhang X, Zhou X, et al. Mechanisms of relapse after CD19 CAR T-cell therapy for acute lymphoblastic leukemia and its prevention and treatment strategies. Front Immunol 2019;10:2664.
5. Blanco B, Ramirez-Fernandez A, Alvarez-Vallina L. Engineering immune cells for in vivo secretion of tumor-specific T cell-redirecting bispecific antibodies. Front Immunol 2020;11:1792.
6. Maude SL, Frey N, Shaw PA, Aplenc R, Barrett DM, Bunin NJ, et al. Chimeric antigen receptor T cells for sustained remissions in leukemia. N Engl J Med 2014; 371:1507–17.
7. Shah NN, Fry TJ. Mechanisms of resistance to CAR T cell therapy. Nat Rev Clin Oncol 2019;16:372–85.
8. Hamieh M, Dobrin A, Cabriolu A, van der Stegen SJC, Giavridis T, Mansilla-Soto J, et al. CAR T cell trogocytosis and cooperative killing regulate tumour antigen escape. Nature 2019;568:112–6.
9. Blanco B, Holliger P, Vile RG, Alvarez-Vallina L. Induction of human T lymphocyte cytotoxicity and inhibition of tumor growth by tumor-specific diabody-based molecules secreted from gene-modified bystander cells. J Immunol 2003;171:1070–7.
10. Compte M, Blanco B, Serrano F, Cuesta AM, Sanz L, Bernad A, et al. Inhibition of tumor growth in vivo by in situ secretion of bispecific anti-CEA x anti-CD3 diabodies from lentivirally transduced human lymphocytes. Cancer Gene Ther 2007;14:380–8.
11. Velasquez MP, Torres D, Iwahori K, Kakarla S, Arber C, Rodriguez-Cruz T, et al. T cells expressing CD19-specific engager molecules for the immunotherapy of CD19-positive malignancies. Sci Rep 2016;6:27130.
12. Liu X, Barrett DM, Jiang S, Fang C, Kalos M, Grupp SA, et al. Improved anti-leukemia activities of adoptively transferred T cells expressing bispecific T-cell engager in mice. Blood Cancer J 2016;6:e430.
13. Castella M, Boronat A, Martin-Ibanez R, Rodriguez V, Sune G, Caballero M, et al. Development of a novel anti-CD19 chimeric antigen receptor: a paradigm for an affordable CAR T cell production at academic institutions. Mol Ther Methods Clin Dev 2019;12:134–44.
14. Haryadi R, Ho S, Kok YJ, Pu HX, Zheng L, Pereira NA, et al. Optimization of heavy chain and light chain signal peptides for high level expression of therapeutic antibodies in CHO cells. PLoS One 2015; 10:e0116878.
15. Compte M, Alvarez-Cienfuegos A, Nunez-Prado N, Sainz-Pastor N, Blanco-Toribio A, Pescador N, et al. Functional comparison of single-chain and two-chain anti-CD3-based bispecific antibodies in gene immunotherapy applications. Oncoimmunology 2014;3:e28810.
16. Zanetti SR, Romecin PA, Vinyoles M, Juan M, Fuster JL, Camos M, et al. Bone marrow MSC from pediatric patients with B-ALL highly immunosuppress T-cell responses but do not compromise CD19-CAR T-cell activity. J Immunother Cancer 2020;8:e001419.
17. Harwood SL, Alvarez-Cienfuegos A, Nunez-Prado N, Compte M, Hernandez-Perez S, Merino N, et al. ATTACK, a novel bispecific T cell-recruiting antibody with trivalent EGFR binding and monovalent CD3 binding for cancer immunotherapy. Oncoimmunology 2017;7:e1377874.
18. Cuesta-Mateos C, Fuentes P, Schrader A, Juarez-Sanchez R, Loscertales J, Mateu-Albero T, et al. CCR7 as a novel therapeutic target in t-cell PROLYMPHOCYTIC leukemia. Biomark Res 2020;8:54.
19. Ortiz-Maldonado V, Rives S, Castella M, Alonso-Saladrigues A, Benitez-Ribas D, Caballero-Banos M, et al. CART19-BE-01: a multicenter trial of ARI-0001 cell therapy in patients with CD19(+) relapsed/refractory malignancies. Mol Ther 2021;29:636–44.
20. Velasco-Hernandez T, Zanetti SR, Roca-Ho H, Gutierrez-Aguera F, Petazzi P, Sanchez-Martinez D, et al. Efficient elimination of primary B-ALL cells in vitro and in vivo using a novel 4-1BB-based CAR targeting a membrane-distal CD22 epitope. J Immunother Cancer 2020; 8:e000896.
21. Graham C, Jozwik A, Pepper A, Benjamin R. Allogeneic CAR-T cells: More than ease of access? Cells 2018;7:155.
22. Majzner RG, Mackall CL. Tumor antigen escape from CAR T-cell therapy. Cancer Discov 2018;8:1219–26.
23. Sapra P, Allen TM. Internalizing antibodies are necessary for improved therapeutic efficacy of antibody-targeted liposomal drugs. Cancer Res 2002; 62:7190–4.
24. Horton HM, Bernett MJ, Pong E, Peipp M, Karki S, Chu SY, et al. Potent in vitro and in vivo activity of an Fc-engineered anti-CD19 monoclonal antibody against lymphoma and leukemia. Cancer Res 2008; 68:8049–57.
25. Du X, Beers R, Fitzgerald DJ, Pastan I. Differential cellular internalization of anti-CD19 and -CD22 immunotoxins results in different cytotoxic activity. Cancer Res 2008;68:6300–5.
26. Scarfo I, Ormhoj M, Frigault MJ, Castano AP, Lorrey S, Bouffard AA, et al. Anti-CD37 chimeric antigen receptor T cells are active against B- and T-cell lymphomas. Blood 2018;132:1495–506.
27. Ormhoj M, Scarfo I, Cabral ML, Bailey SR, Lorrey SJ, Bouffard AA, et al. Chimeric antigen receptor T cells targeting CD79b show efficacy in lymphoma with or without cotargeting CD19. Clin Cancer Res 2019;25: 7046–57.
28. Liu H, Rhodes M, Wiest DL, Vignali DA. On the dynamics of TCR:CD3 complex cell surface expression and downmodulation. Immunity 2000;13: 665–75.
29. Li W, Qiu S, Chen J, Jiang S, Chen W, Jiang J, et al. Chimeric antigen receptor designed to prevent ubiquitination and downregulation showed durable anti-tumor efficacy. Immunity 2020;53:456–70.
30. Davenport AJ, Jenkins MR, Cross RS, Yong CS, Prince HM, Ritchie DS, et al. CAR-T cells inflict sequential killing of multiple tumor target cells. Cancer Immunol Res 2015;3:483–94.
31. Walker AJ, Majzner RG, Zhang L, Wanhainen K, Long AH, Nguyen SM, et al. Tumor antigen and receptor densities regulate efficacy of a chimeric

antigen receptor targeting anaplastic lymphoma kinase. Mol Ther 2017;25:2189–201.
32. Mukherjee M, Mace EM, Carisey AF, Ahmed N, Orange JS. Quantitative imaging approaches to study the CAR immunological synapse. Mol Ther 2017;25:1757–68.
33. Davenport AJ, Cross RS, Watson KA, Liao Y, Shi W, Prince HM, et al. Chimeric antigen receptor T cells form nonclassical and potent immune synapses driving rapid cytotoxicity. Proc Natl Acad Sci U S A 2018;115:E2068–76.
34. Watanabe K, Kuramitsu S, Posey AD Jr, June CH. Expanding the therapeutic window for CAR T cell therapy in solid tumors: the knowns and unknowns of CAR T cell biology. Front Immunol 2018;9:2486.
35. Offner S, Hofmeister R, Romaniuk A, Kufer P, Baeuerle PA. Induction of regular cytolytic T cell synapses by bispecific single-chain antibody constructs on MHC class I-negative tumor cells. Mol Immunol 2006;43:763–71.
36. Kouhestani D, Geis M, Alsouri S, Bumm TGP, Einsele H, Sauer M, et al. Variant signaling topology at the cancer cell-T-cell interface induced by a two-component T-cell engager. Cell Mol Immunol 2021;18:1568–70.